KTH ROYAL INSTITUTE
OF TECHNOLOGY

Degree Project In Solid Mechanics

Second Cycle 30 Credits

# In-plane bi-axial testing of thin paper

**ASAD ALI**

**DANAY MICHAEL**

Stockholm, Sweden 2022

# Abstract

During its lifetime, a beverage package is subjected to a complex loading history where the loading, in general, is multiaxial. Hence, to optimize the performance of the package, knowledge of the material's anisotropic multi-axial deformation and subsequent failure is necessary. This report presents a way to investigate the anisotropic loading and fracture of thin paper using bi-axial testing and to analyse the bi-axial test using the Finite Element Method.

Getting thin paper to fracture in the central region, where the deformation and loading are bi-axial, proved difficult. To overcome this challenge, a new bi-axial specimen, with a specific sample preparation technique, is proposed and implemented in this specific project. This cruciform-shaped thin paper specimen was reinforced with laminating plastic everywhere but in the central region. This was done to avoid material failure in the notched radius area or the clamps, rather to facilitate a material failure in the central region of the material specimen. In order to simulate the bi-axial test, a Hill elastic-plastic material model was calibrated, and the material parameters were obtained from uniaxial tensile tests.

When subjected to bi-axial loading, the proposed cruciform-shaped specimen fractured systematically and repetitively for the different load cases studied. Moreover, the Hill material model captured the force vs. displacement curve from the experimental results well but overestimated its values. The overestimation was mainly due to sliding during the experimental tests.

# Sammanfattning

Under sin livstid utsätts en kartongförpackning för olika fleraxliga belastningar. Därför är det viktigt att ha bättre förståelse för materialets anisotropa brottbeteende för att kunna optimera förpackningens prestanda. Detta projekt fokuserar på att hitta en metod för att undersöka brott av ett tunt papper under fleraxlig belastning med hjälp av bi-axiella dragprov och därefter simulera det bi-axiella provet med finita element-metoden.

Det har visat sig vara svårt att få tunt papper gå sönder i de områden av provstavar där spänningstillståndet kan beskrivas som bi-axiellt. Oftast sker brott vid spänningskoncentrationer. För att komma runt denna utmaning föreslås en ny bi-axiell provstav. I denna är provstaven förstärkt med laminerad plast överallt förutom i mitten där det önskvärda spänningstillståndet råder. För att simulera det bi-axiella dragprovet, kalibrerades Hills elastiskt-plastiska materialmodell och materialparametrarna bestämdes med hjälp av enaxlig dragprov.

Den designade provstaven utsättes för olika bi-axiella laster och brott initierades på rätt ställe i provstaven på ett systematiskt och repeterbart sätt. Kraft-förskjutningskurvan från experimenten kunde beskrivas väl av simuleringarna, men värdet på kraften överskattades. Detta på grund av glidning mellan provstaven och greppet under försöken i den bi-axiella provningsmaskinen.

# Preface

First and foremost, we would like to thank our supervisor and examiner, Prof. Sören Östlund, for his invaluable insights, help, and feedback throughout the thesis work. We would also like to thank our supervisors at Tetra Pak, Eskil Andreasson and Anders Harrysson, for their supervision and fruitful discussions during the process. A very special thanks to Eskil for his enthusiasm and guidance, not the least regarding the presentation of the results.

We would also like to thank Ph.D. student Mossab Alzweighi for his help with the experimental tests and express our deepest gratitude to Prof. Artem Kulachenko for his expertise in FEM modelling and for always taking his time to answer our questions.

Finally, we wish to extend our thanks to our families and friends for their great support and encouragement, and lastly, a big thanks to our friend Khashaiar, who made life at KTH more fun.

# Contents

# List of Figures

# List of Tables

# 1 Introduction

## 1.1 Paper as an engineering material

Paper and paperboard are two materials commonly used in the process industry, more so in the packaging industry. This is due to their relatively low cost, high recyclability, renewabilty, good strength-to-weight ratio and stiffness-to-weight ratios [10]. However, due to the increasing competition in the market, the producers of packaging materials are forced to develop and improve their products constantly [14]. This leads to a desire to have paper and paperboard with improved strength properties, which is important not only in the paper industry but also of great interest to the fields of packaging and light-weight building material [7].

Paper is made up of a network of pressed cellulose fibers which are derived from wood by mechanical or chemical pulping. The various methods give different properties of fibers which affect the properties of paper products. The typical fiber dimensions are 1-5 mm in length and 20-50 µm in width [12]. The mechanical characterization of paper at different structural levels is illustrated in Figure 1.

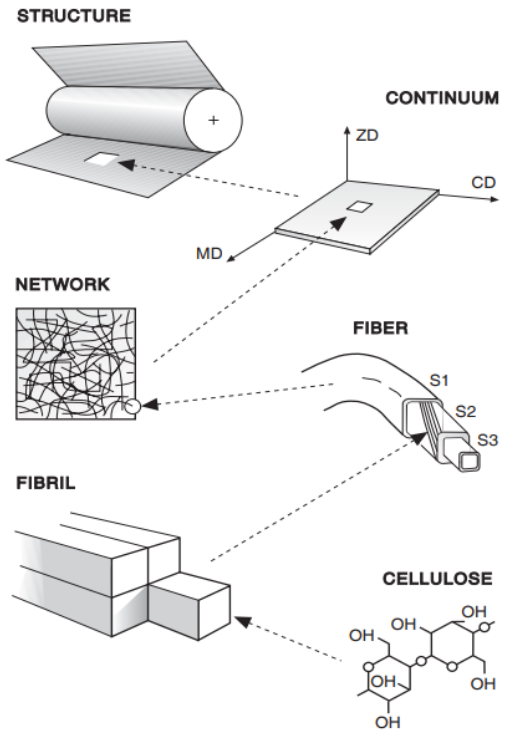


Figure 1: Characterization of paperboard at different structural levels [16].

During paper and paperboard production, the pulp is diluted with a water solution containing fibers and distributed onto a moving water-permeable fabric. As the fabric moves, the water-fibers solution is drained, causing the fibers to stack- and align in the flow direction to form paper, followed by pressing- and drying [3]. This process gives the paper and paperboard their anisotropic mechanical properties. On a macroscopic level, paper and paperboard can, to a good approximation, be described as orthotropic with different mechanical properties in the three principal directions, machine direction (MD), cross direction (CD), and out-of-plane (or through-thickness) direction (ZD), see Figure 2. Stacking the fibers on top of each other makes the mechanical properties in MD-CD plane 100 times higher than the mechanical properties in ZD [3].

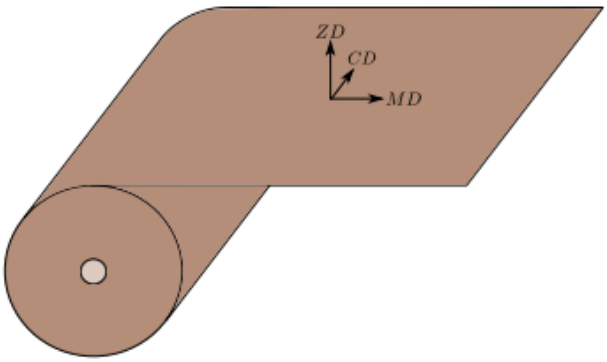


Figure 2: The three principal material directions of paper and paperboard [2].

During its lifetime, a beverage package is subjected to a complex loading history where the loading, in general, is multiaxial. This might, for instance, occur as early as in production, when a piece of paperboard is subjected to in-plane loads and sometimes also three-dimensional loading state, i.e., during drying. Multiaxial stress state and strain rates might also arise during 3-D forming operations when the paperboard is converted to a package. Creasing, hydroforming, embossing, press forming, and deep drawing are all operations that cause bi-axial and, in certain instances, tri-axial stress and strain states. Moreover, after production, the package can still be subjected to multi-axial loading and these can arise from transport loads, and also during usage by the customer [10].

Hence, to optimize the performance of the package, knowledge of material properties due to the variety of bi-axial stress and strain states that the package is subjected to its lifetime is needed. The uniaxial tensile test is widely used to char-

acterize the failure properties due to its low cost and simplicity. However, bi-axial test methods are needed when the material is subjected to multi-axial stress state. The two most widely used bi-axial methods in previous work are testing on tubular specimens and cruciform specimens. De Ruvo et al.[5] utilized the bi-axial test on tubular specimens, which were subjected to axial loading, internal pressure and torsional loading simultaneously to determine the failure envelope of paper. Gunderson et al. [6] performed in-plane bi-axial tests on cruciform specimens to get the failure surface for paperboard.

Bi-axial testing using cruciform specimen is a traditionally preferred method if yield- or failure surface is desired due to its ease of producing a bi-axial stress state. This is obtained by varying the displacement or the ratio of the load imposed on the axes. However, this method has an intrinsic disadvantage: it is difficult to deform the region experiencing bi-axial deformation and loading to the fracture point. As a result, failure occurs in the arms of the cruciform specimen. Bi-axial metal and composite specimens are weakened in the central region through thickness reduction by milling to overcome this challenge [10]. In doing so, the center region will have a homogeneous stress state; hence strain localization or failure will occur in that region. However, this method of milling the specimen has the limitation that it causes stress concentrations in the specimen. Linvill et al. [10], in their research proposed and implemented a new bi-axial testing method to get the failure to initiate in the center region of the paperboard. They designed a new specimen, where three quarters of the material thickness was removed with a laser cutter in the center region. They used the proposed method to study the stress- and strain-based yield- and failure surfaces for paperboard.

## 1.2 Objectives

The purpose of this thesis was to contribute to the optimization of the performance of the package through improved knowledge building of material properties of a thin paper during anisotropic failure. The intended outcomes of this thesis are:

- Propose and implement a new bi-axial testing method for thin paper.
- Experimentally investigate the anisotropic properties of failure in thin paper using bi-axial testing.
- Calibrate material model using finite element simulation.

# 2 Experiments

Both bi-axial and uniaxial experiments were performed during this thesis to evaluate the anisotropic failure properties of thin paper. This section presents the procedures followed to perform the experiments. All the experiments were performed at 23°C and 50% RH.

## 2.1 Bi-axial testing

To determine the multi-axial failure properties of thin paper, bi-axial tensile tests were performed. Cruciform shaped specimen was used, allowing the in-plane deformation of the material under different loading conditions [3]. The bi-axial machine used was a Zwick D07144425. The testing machine has four actuators, each with a capacity of 1kN. The two in-plane principal directions, MD and CD, coincide with the loading directions. Two opposing axes were clamped to the end of the specimen in the MD, and the other two axes were clamped to the end of the specimen in the CD, as illustrated in Figure 3a. The cruciform geometry and its dimensions are shown in Figure 3b. To avoid damaging the thin paper and to have more precise dimensions, a laser cutting machine was used to prepare the cruciform specimen. A video camera is mounted above the specimen to film the test, as shown in Figure 3c. The image sequence acquired from the test can be used to calculate the experimental strains using the Digital Image correlation (DIC) technique.

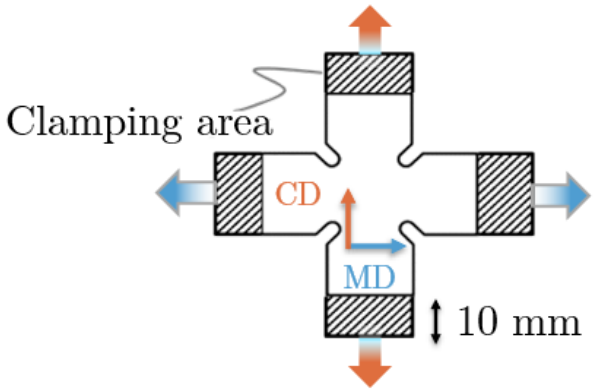


(a) *Bi-axial specimen set-up*

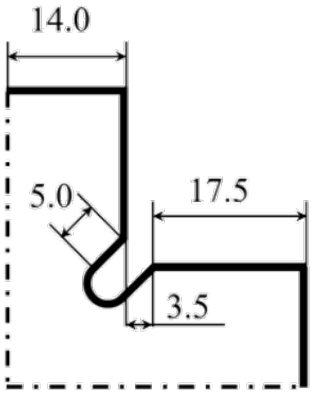


(b) *Bi-axial specimen dimensions [mm]*

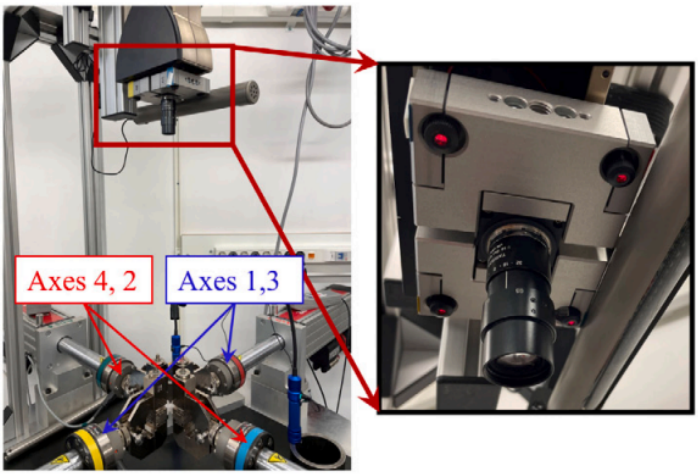


(c) *Bi-axial testing machine [3]*

Figure 3: Experimental setup for bi-axial tensile tests

Since the material of interest is very thin, when the cruciform specimen in Figure 3a is subjected to bi-axial loading conditions, failure occurs at the notch and not the region experiencing a bi-axial stress state as seen in Figure 4.

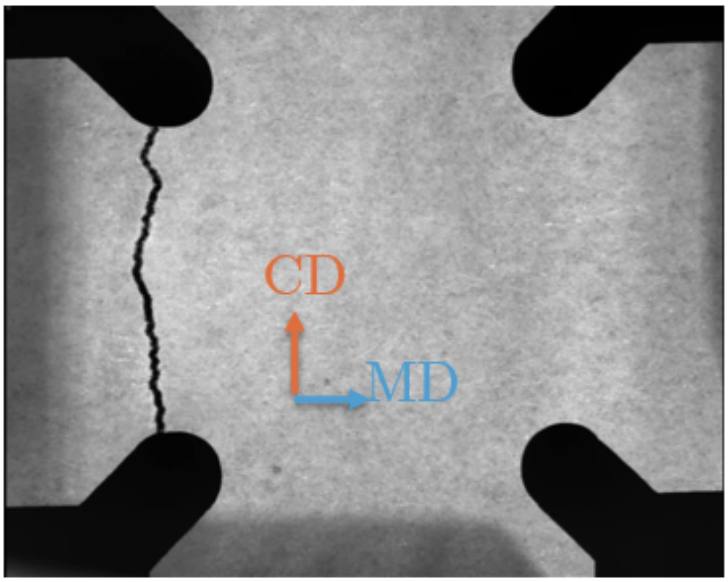


Figure 4: Failure in thin paper

It is desirable to find a specimen where the localization and failure occur in the center where there is a state of bi-axial deformation and loading. To overcome this challenge, the material can be weakened in the region of interest by either milling or laser engraving [10]. Since the paper of study in this thesis is very thin, removing some material in the center is not possible because the material would be damaged. To increase the probability that failure initiates in the central region, the thin paper is strengthened in the other regions. This is done by laminating the cruciform-shaped paper specimen with a polymer material with a circular hole in the middle on both sides of the thin paper as illustrated in Figure 5.

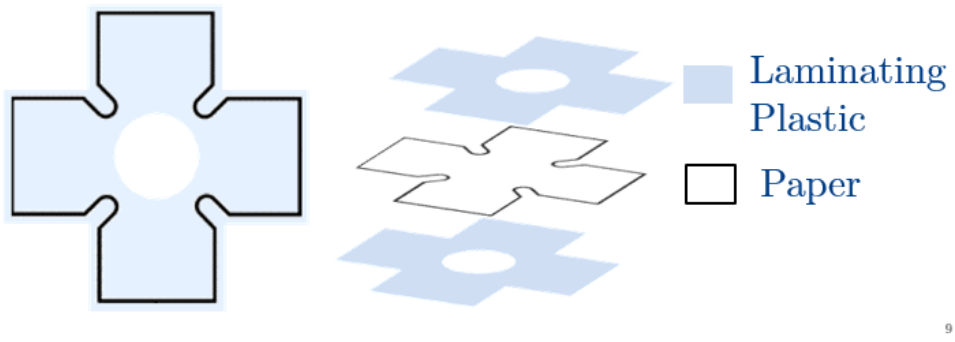


Figure 5: Design of laminated bi-axial specimen for thin paper

### 2.1.1 Specimen preparation

First circular holes with a diameter 24 mm were cut out from a double-layered polymer material of size A4. The cruciform-shaped thin paper is then placed between the two plastic layers and aligned so that the hole is placed in the central region of the paper. Here, the MD of the paper was always aligned with the longitudinal direction of the laminating plastic. Next, a laminating machine Lamiart 3201, was used to bond the two plastic layers onto the paper. Lastly, the composite made of paper with two layers of laminating plastic is cut into pieces with a scissor and kept at 23 °C and 50 % for at least 24 hours before testing. The whole process of specimen preparation is illustrated in Figure 6.

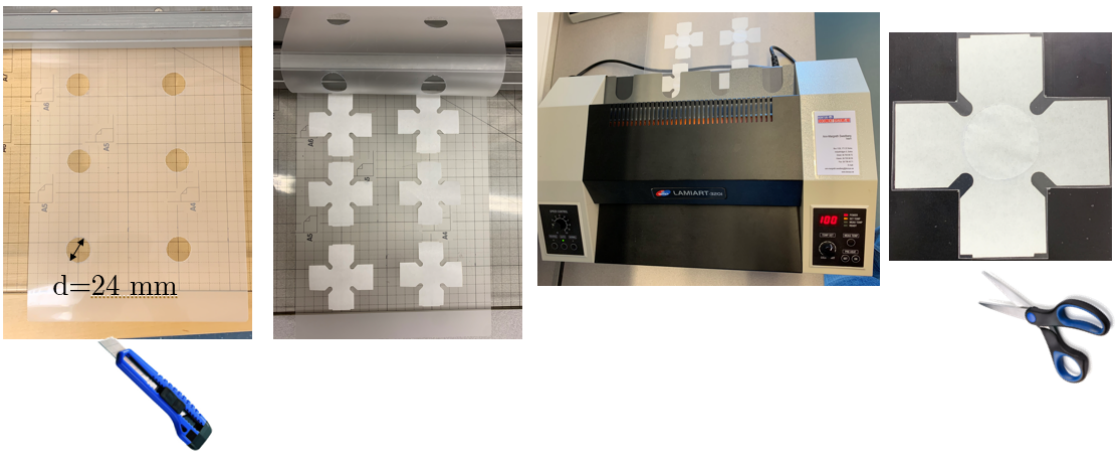


Figure 6: Bi-axial specimen preparation

### 2.1.2 Bi-axial tensile testing of laminated paper

The two in-plane principal directions, MD and CD of the laminated paper, coincide with the loading directions. The two opposing axes were clamped to the end of the specimen in MD, and the other two were clamped to the end of the specimen in the CD, as illustrated in Figure 7. In all the tests, the opposing axes move simultaneously. This prevents shifting of the mid of the specimen during bi-axial loading [3].

The material was subjected to different loading conditions by imposing different displacement-rate ratios along the axis coinciding with MD- and CD. Table 1 shows the different displacement-rate ratios studied.

Table 1: Displacement-rate ratios studied

| **Test number** | **1** | **2** | **3** |
|---|---|---|---|
| Displacement ratio ($v_{MD}$ (mm/min)/$v_{CD}$ (mm/min)) | 3/3 | 6/3 | 3/6 |

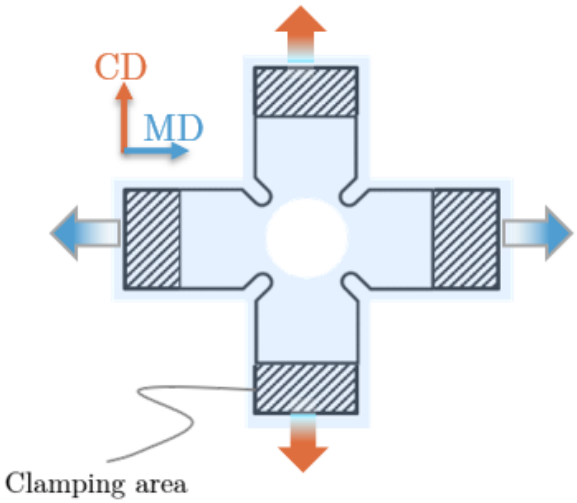


Figure 7: Bi-axial specimen set-up

## 2.2 Uniaxial tensile test

To derive the mechanical properties of the material, uniaxial tensile tests were performed for both the thin paper and one layer- of the laminating plastic. To capture the in-plane properties of the thin paper, the tests were performed in three directions, MD, CD and a 45° bisecting MD and CD. The strips of the thin paper used in the tests were cut out using a paper cutter, see Figure 8a. The dimensions of the uniaxial specimen for the paper were 100 × 15 mm. To see if the plastic shows anisotropic behavior, tests were performed in the three directions, MD, CD and 45°. Here, MD was chosen as the longitudinal direction. The plastic specimen used in the uniaxial tensile tests had the same dimensions as the thin paper but with a thickness of 175 µm.

The tests were performed under displacement control using the same testing machine used in the bi-axial tests, see Figure 8b. The displacement rate was set to 3 mm/min for all tests. Ten tests were done along each direction, and force vs. displacement curves were captured and later processed and analyzed using MATLAB [11].

The material characterization can also be done using a bi-axial tensile test. However, due to the inhomogeneity of the stresses and the strains in the cruciform specimen, this procedure is not only cumbersome but also requires inverse parameter identification [3].

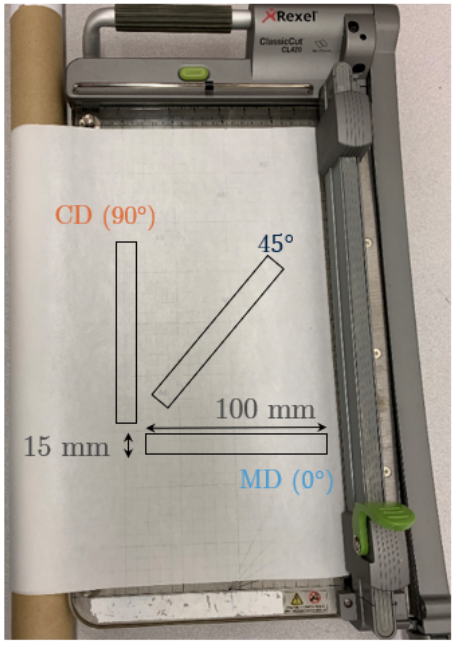


(a) *uniaxial tensile specimen*

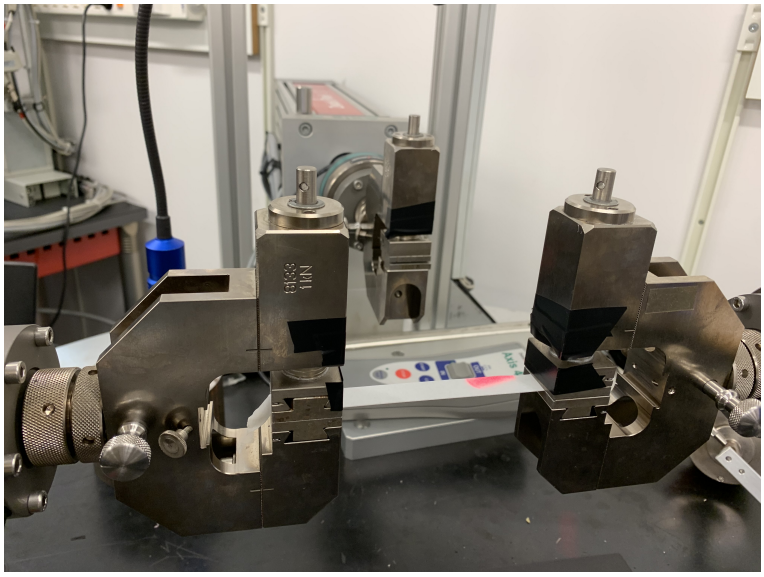

(b) *Uniaxial tensile specimen mounting*

Figure 8: Experimental set-up for uniaxial tensile tets

## 2.3 Digital image correlation

Slippage in the clamps is something that can not be avoided entirely. The effect of slippage can be accounted for if one uses Digital Image Correlation, DIC, to measure strains. DIC is also a necessity when local strains are of interest. DIC is a non-contacting strain measurement that uses the natural pattern of the material or an applied speckle pattern if the material lacks such a pattern to measure local strains [15]. DIC measurements are performed by taking an image sequence during the experiment. Then, by using the undeformed image as a reference image, the displacement of the pattern in the deformed images can be identified by correlating the image sequence with the reference image. The process is illustrated in Figure 9.

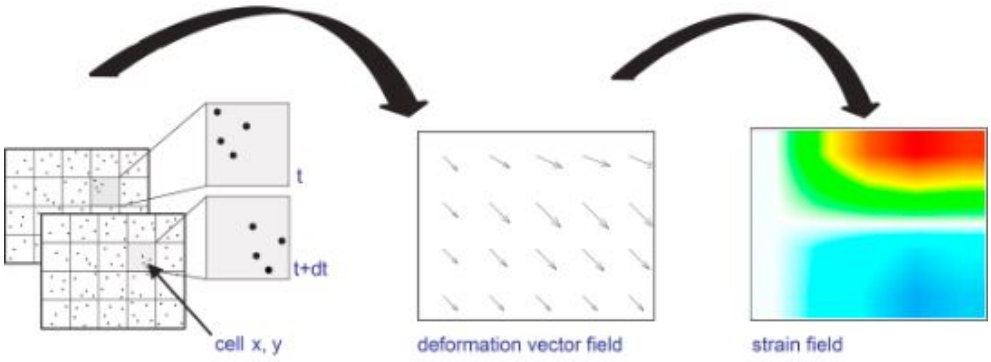


Figure 9: The process of DIC [8]

The material used in this experiment lacked a natural pattern. Therefore, some patterns had to be created. Moreover, the polymer part of the specimen reflected the lights and was too shiny; therefore, something had to be done to avoid it. Since the paper was white, applying some black speckles was enough. As for the polymer material, it was first coated with thin white paint before black speckles could be applied on top of it. The speckle pattern on the specimen is shown in Figure 10.

As can be seen in Figure 3c, one video camera, which is mounted above the specimen, was used to capture the image sequences. The image sequences acquired from the test was then used to calculate the experimental displacement using the software program VIC-2D [17]. The distance between the clamps in both MD and CD is 50 mm. However, the field of view of the camera was lower than that. Hence, two points are chosen, and their displacements are tracked over time. The points chosen are the top and right end points of the specimen, which can be seen

in Figure 10 marked as red squares. These displacements were then compared with the directional displacement of their corresponding points in the FE simulation. The directional displacement in CD was followed at the point in the upper end, while the directional displacement in MD was followed at the point in the right end of the specimen. Only two points were chosen to account for slippage. This is based on the assumption that slippage on the opposite clamp should be equal since the applied loads, material properties, and specimen dimensions were the same.

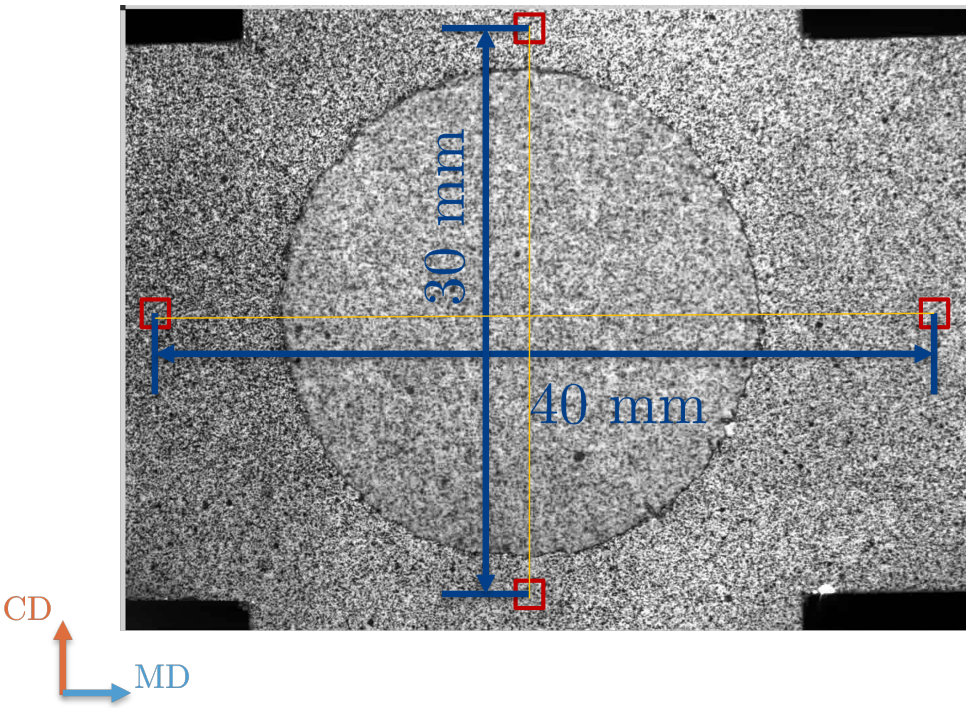


Figure 10: DIC set-up

# 3 Constitutive modelling

In this chapter, the constitutive modelling theory is presented.

## 3.1 Linear elasticity

For an orthotropic material like paper, Hooke's law is valid for linear elasticity and can, in tensor form, be expressed as

$$\boldsymbol{\varepsilon^e} = \boldsymbol{C\sigma}, \tag{1}$$

which when expanded can be written as

$$\begin{bmatrix} \varepsilon^e_{11} \\ \varepsilon^e_{22} \\ \varepsilon^e_{33} \\ 2\varepsilon^e_{12} \\ 2\varepsilon^e_{13} \\ 2\varepsilon^e_{23} \end{bmatrix} = \begin{bmatrix} \frac{1}{E_1} & -\frac{v_{21}}{E_2} & -\frac{v_{31}}{E_3} & 0 & 0 & 0 \\ -\frac{v_{12}}{E_1} & \frac{1}{E_2} & -\frac{v_{32}}{E_3} & 0 & 0 & 0 \\ -\frac{v_{13}}{E_1} & -\frac{v_{23}}{E_2} & -\frac{1}{E_3} & 0 & 0 & 0 \\ 0 & 0 & 0 & \frac{1}{G_{12}} & 0 & 0 \\ 0 & 0 & 0 & 0 & \frac{1}{G_{13}} & 0 \\ 0 & 0 & 0 & 0 & 0 & \frac{1}{G_{23}} \end{bmatrix} \begin{bmatrix} \sigma_{11} \\ \sigma_{22} \\ \sigma_{33} \\ \sigma_{12} \\ \sigma_{13} \\ \sigma_{23} \end{bmatrix}, \tag{2}$$

Here, indices 1,2 and 3 denote the three orthogonal principal material directions. For paper materials, it corresponds to MD, CD and ZD. Moreover, $E_{ij}$ are Young's moduli, $v_{ij}$ are Poisson's ratios, and $G_{ij}$ are the shear moduli for $i, j$ =1,2,3.

For plane stress conditions, Eq. (2) can be reduced to

$$\begin{bmatrix} \varepsilon^e_{11} \\ \varepsilon^e_{22} \\ 2\varepsilon^e_{12} \end{bmatrix} = \begin{bmatrix} \frac{1}{E_1} & -\frac{v_{21}}{E_2} & 0 \\ -\frac{v_{12}}{E_1} & \frac{1}{E_2} & 0 \\ 0 & 0 & \frac{1}{G_{12}} \end{bmatrix} \begin{bmatrix} \sigma_{11} \\ \sigma_{22} \\ \sigma_{12} \end{bmatrix}. \tag{3}$$

The compliance matrix $\boldsymbol{C}$ is symmetric, which gives the following relation

$$\frac{v_{12}}{E_1} = \frac{v_{21}}{E_2} \tag{4}$$

The parameters $v_{12}$, $v_{21}$ and $G_{12}$ are difficult to determine experimentally; hence a good approximation is needed. From empirical observations [4], it is found that

$$v_{12} = 0.293\sqrt{\frac{E_1}{E_2}} \tag{5}$$

is a good approximation. Moreover, the in-plane shear modulus $G_{12}$ can be approximated using [9] as

$$G_{12} = \left( \frac{4}{E_{45}} - \frac{1}{E_1} - \frac{1}{E_2} + \frac{2v_{12}}{E_1} \right)^{-1} \tag{6}$$

## 3.2 Plasticity

The relations in Eqs. (2)-(6) are only applicable during elastic loading, i.e., when the material recovers to its original configuration when unloaded. The material behaves linearly until the initial yield stress, $\sigma_{y_0}$, is reached, and after that, plastic strain is developed. After the initial yielding, the stress increases with increasing strain and unloading at point A, see Figure 11, to point B occurs elastically with Young's modulus, $E$. The total strain at point A is a superposition of the elastic strains $\varepsilon^e$ and plastic strains $\varepsilon^p$.

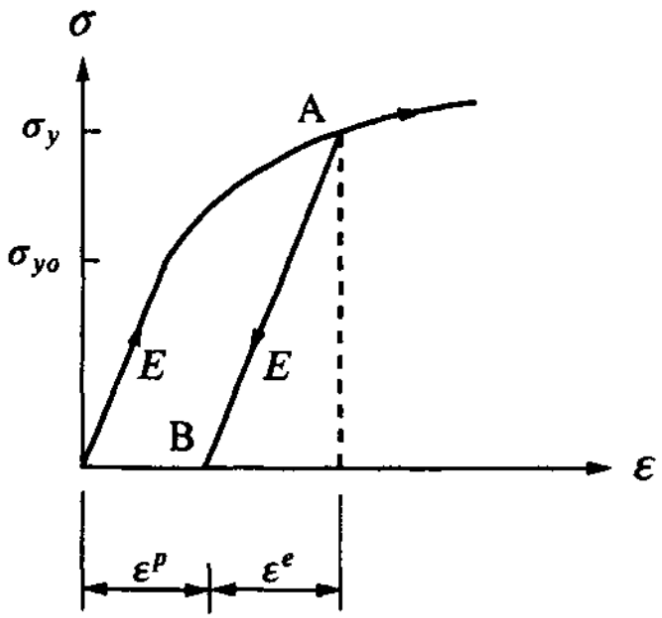


Figure 11: Strain-strain curve for elastic-plastic material [13].

To distinguish if the material has undergone plastic deformation or not, a yield function, $f$, is needed. The yield function, $f < 0$ for linear elastic deformation and $f = 0$ when the initial yield stress has been reached, and plasticity deformation occurs. The yield function, $f$, can be stated as

$$f(\sigma_{ij}, K_\alpha) = 0, \tag{7}$$

where $\sigma_{ij}$ and $K_\alpha$ denote the in-plane stress tensor and the hardening parameters, respectively [13]. By introducing internal variables, $k_\beta$, which characterize the elasto-plastic material, the following assumption can be made

$$K_\alpha = K_\alpha(k_\beta) \tag{8}$$

Consequently, from Eq. (9), it follows that

$$\dot{K}_\alpha = \frac{\partial K_\alpha}{\partial k_\beta}\dot{k}_\beta \tag{9}$$

here, a dot above the variables denotes the rate, i.e., the change with respect to time.

As mentioned, the internal parameters $k_\beta$ characterize the elastic-plastic material and hence can only change during plastic loading, which leads to

$$\dot{k}_\beta = \dot{K}_\alpha = 0 \quad \text{for elastic behaviour.} \tag{10}$$

During plastic loading $f = 0$; therefore, the consistency relation $\dot{f} = 0$ holds which, with Eq. (7) and chain rule, results in

$$\frac{\partial f}{\partial \sigma_{ij}}\dot{\sigma}_{ij} + \frac{\partial f}{\partial K_\alpha}\dot{K}_\alpha = 0, \tag{11}$$

where $\dot{K}_\alpha$ is defined in Eq. (9).
The evolution of plastic strains is obtained from the associative flow rule as

$$\dot{\epsilon}^p_{ij} = \dot{\lambda}\frac{\partial f}{\partial \sigma_{ij}}; \quad \dot{\lambda} \geq 0 \tag{12}$$

where $\dot{\lambda}$ is the plastic multiplier. Moreover, for incremental plasticity, the rate of internal variables is proportional to the plastic strain rate multiplier and can be expressed as

$$\dot{k}_\alpha = \dot{\lambda} k_\alpha(\sigma_{ij}, K_\beta) \tag{13}$$

where $k_\alpha$ denotes the evolution functions determined experimentally or through assumptions. From the laws of thermodynamics, it is found out that

$$\dot{k}_\alpha = -\dot{\lambda}\frac{\partial f}{\partial K_\alpha}, \tag{14}$$

The consistency relation can now be expressed as

$$\frac{\partial f}{\partial \sigma_{ij}}\dot{\sigma}_{ij} - H\dot{\lambda} = 0 \tag{15}$$

where $H$ is called the generalized plastic modulus and is expressed as

$$H = -\frac{\partial f}{\partial K_\alpha}\frac{\partial K_\alpha}{\partial k_\beta}k_\beta \tag{16}$$

### 3.2.1 Hill's yield criterion

To account for the anisotropy effects of the paper, a yield function is needed. In this thesis, Hill's yield criterion is considered. It can be formulated as,

$$f = \sigma_{eq}^2 - \sigma_y^2(k), \tag{17}$$

where $\sigma_{eq}$, $\sigma_y$ and $k$ are the equivalent stress, hardening function, and hardening parameter, respectively [3]. The equivalent stress is expressed as

$$\sigma_{eq} = \sqrt{\frac{1}{2}\boldsymbol{\sigma}^{\boldsymbol{T}}\boldsymbol{P}\boldsymbol{\sigma}}, \tag{18}$$

where, $\boldsymbol{\sigma}$ is the stress vector. Since the material, in this case, is very thin and exposed to in-plane loads, plane stress conditions are assumed. Hence, the stress vector can be written as; $\boldsymbol{\sigma} = [\sigma_{11}, \sigma_{22}, \sigma_{12}]^T$. Here, indices 1,2 denote the two principal directions, MD and CD, while 12 denotes the in-plane shear direction. In Eq. (18), $\boldsymbol{P}$ is the orthotropic plastic matrix, and it describes the anisotropy of the material. By choosing the 2-direction as a reference direction, the yield ratio in the 2-direction,$R_{22}$, equals 1, and by setting $R_{33} = 1$, the plastic matrix can be formulated as,

$$\boldsymbol{P} = 2\begin{bmatrix} \frac{1}{R_{11}^2} & \frac{-1}{2R_{11}^2} & 0 \\ \frac{-1}{2R_{11}^2} & 1 & 0 \\ 0 & 0 & \frac{3}{R_{12}^2} \end{bmatrix}, \tag{19}$$

where $R_{11}$, $R_{11}$ and $R_{12}$ are anisotropic yield stress ratios.

For the second term in Eq. (17), isotropic hardening is used, which can be expressed as,

$$\sigma_y(\kappa) = \sigma_0 + H_0\kappa^{\frac{1}{n}}, \tag{20}$$

where $\sigma_0$, $H_0$- and $n$ are the initial yield stress, hardening modulus, and hardening

exponent, respectively. The hardening parameter, $\kappa$, is equal to the equivalent plastic strain, $\kappa = \epsilon^p_{eq}$ or $\dot{\kappa} = \dot{\epsilon}^p_{eq}$, where $\dot{\epsilon}^p_{eq}$ is the equivalent plastic strain rate is expressed as

$$\dot{\epsilon^p_{eq}} = \sqrt{\frac{2}{3}(\dot{\epsilon^p})^T \dot{\epsilon^p}}, \tag{21}$$

here, the plastic strain rate vector; $\dot{\epsilon^p} = [\dot{\epsilon^p_{11}}, \dot{\epsilon^p_{22}}, \dot{\epsilon^p_{12}}]^T$. The evolution of plastic strain is defined in Eq (12).

# 4 Finite-element simulation

FE-simulation of the uniaxial tensile test was first performed to calibrate the material model, which was later used in the biaxial test simulations. The material model used is developed by Alzweighi, from the department of Solid Mechanics at KTH, based on Hill Plasticity which is presented in chapter 3 [3]. All the simulations were carried out in ANSYS Workbench 2020 R2 [1]. The MD and CD of the paper and polymer material were chosen to coincide with the $x$- respective $y$-direction of the FE-model.

## 4.1 Uniaxial test simulation

The same setup and geometry dimensions were used in the FE-model as in the experimental to obtain similar results. It was modelled as a plane stress problem since the geometry was very thin and no out-of-plane forces were acting on the the model's surface. The mesh element size was set to be $3 \times 3$ mm as shown in Figure 12. The load was applied as a prescribed displacement $u$, on the upper end while the lower end was constrained in all directions.

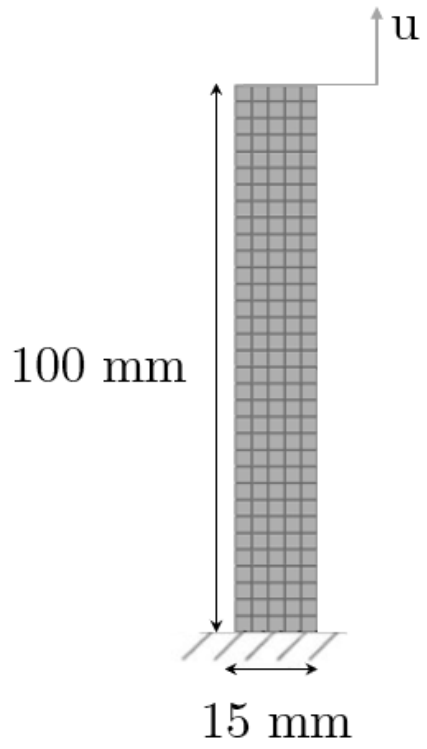


Figure 12: Uniaxial model used in FE simulations.

To calibrate the material model, the CD was chosen as the reference direction. Hence $R_{yy}$ was set to be 1. CD was chosen as the reference direction simply due to the larger deformation than the other two directions, hence better calibration. The initial yield stress, $\sigma_0$, the hardening modulus, $H_0$, and the hardening exponent, $n$, were calibrated from the CD. Moreover, $R_{zz}$ was set to 1 as it did not affect the fitting accuracy. The remaining material parameter, $R_{xx}$, was determined by rotating the model 90° around the $z$-axis so that the loading direction coincided with the MD. It was then varied until the stress-strain curve obtained from FE analysis fitted the experimental results. The same procedure was followed to determine $R_{xy}$, except that the geometry was now rotated 45° and loaded in that direction.

## 4.2 Bi-axial test simulation

3D-shell elements were used to model the geometry in the bi-axial simulations. The specimen was was modelled as a one shell composite with three sections, as illustrated in Figure 13.

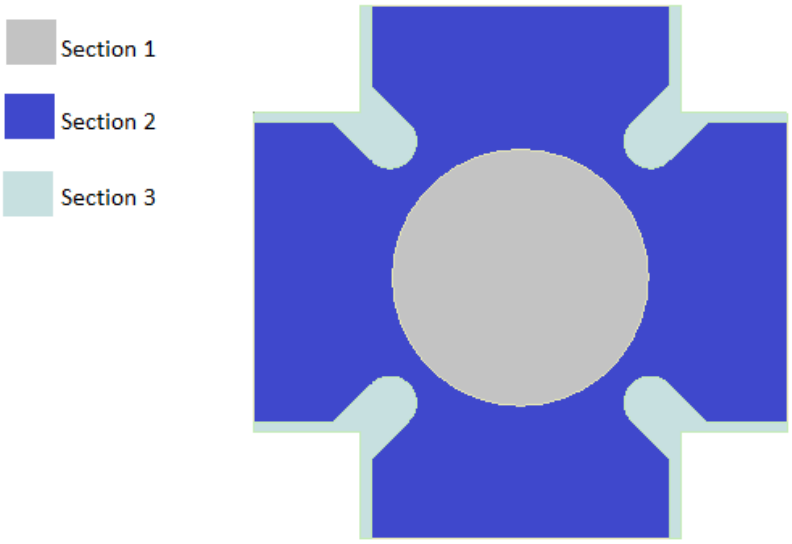


Figure 13: Bi-axial model used in the FE simulations.

Elasto-plasticity is assumed, where the material is characetrized by orthotropic linear elastic response and non-linear plastic response. The material parameters are obtained from the uniaxial tensile tests and Hill's material model was employed to capture the non-linear material response.

Section one consisted of one layer and was assigned the material model calibrated for the paper. The second section consisted of three layers, where the top- and bottom layers were assigned the material model calibrated for the plastic, while the middle layer was assigned the same material model as section one. The third section consisted of two layers and both layers were the plastic material model.

Similar to the uniaxial simulation tests, the loads were applied as a displacement on the four edges. By imposing different displacements on both axes, the different load cases tested in the experiments presented in chapter 2 could be simulated. Following the experiments, the three load cases are stated in Table 2.

Table 2: Displacement ratios simulated

| **Test number** | **1** | **2** | **3** |
|---|---|---|---|
| Displacement ($U_{MD}$ (mm)/$U_{CD}$ (mm)) | 0.6/0.6 | 0.6/0.3 | 0.6/1.2 |

# 5 Results

## 5.1 Biaxial testing

When subjected to in-plane bi-axial loading, the designed cruciform specimen failed systematically and repetitively for each load case. Fracture was initiated in the central region of the cruciform specimen and then propagated towards the edges at a certain angle depending on the load case, as illustrated with one example in Figure 14. In the illustrated example, the displacements and the displacement rates were twice as large in CD than in MD.

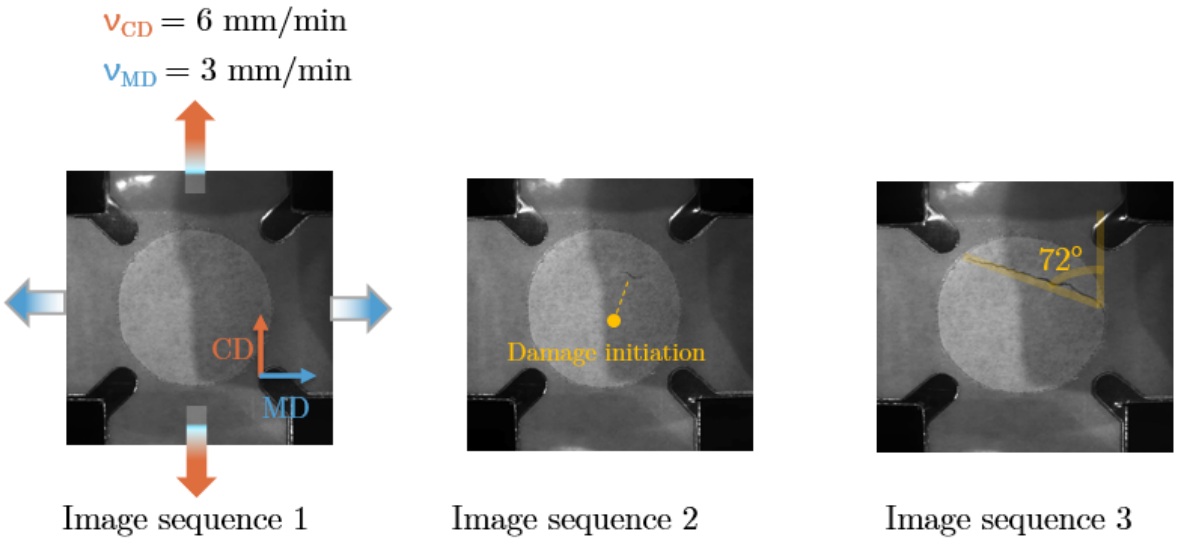


Figure 14: Failure initiation and propagation for the load case $v_{CD} = 2v_{MD}$

In Figure 15, a representation of how the failure was orientated for each load case is illustrated. More tests were done for each load case and the failure orientation of each load case is illustrated in Appendix B.

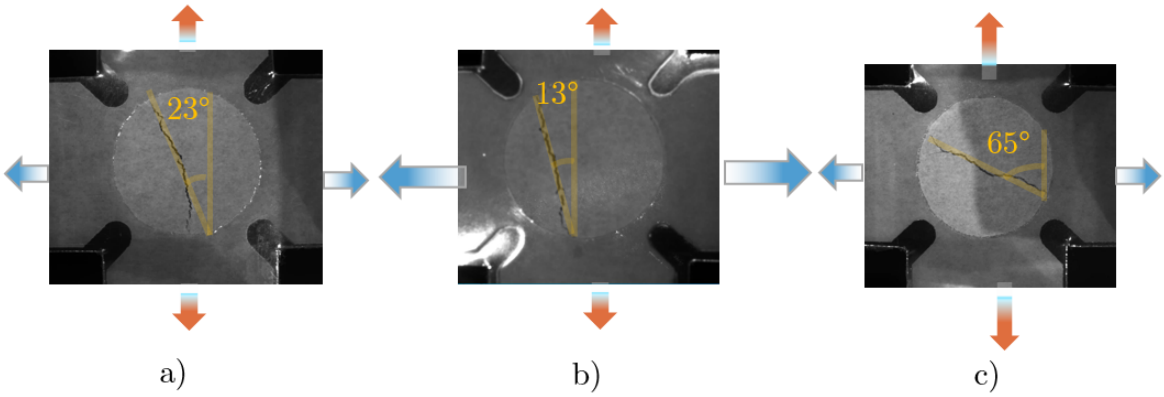


Figure 15: Fracture path orientation for the different load cases. a) $v_{MD} = v_{CD}$, b) $v_{MD} = 2v_{CD}$ and c) $v_{CD} = 2v_{MD}$

The failure propagated at a certain angle with small variation for the different load cases. The mean value and the standard deviation for the different load cases are presented in Figure 16.

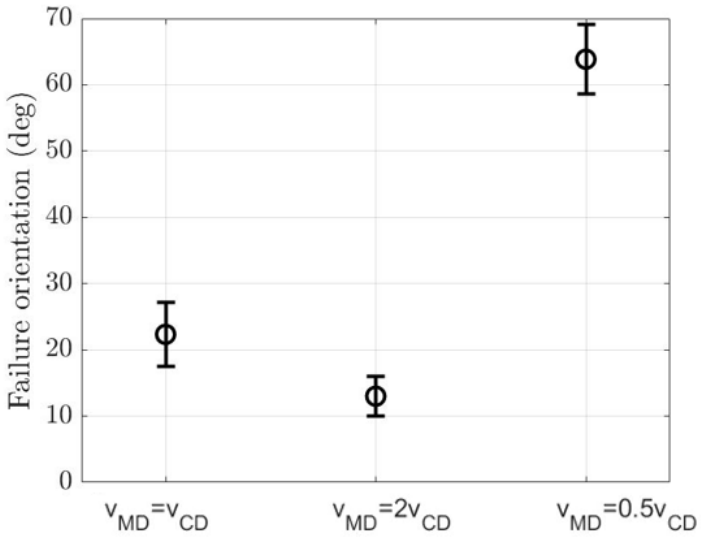


Figure 16: Failure orientation for the different load cases

## 5.2 Material model calibration

Ten uniaxial tests were conducted in each direction for the material characterization of paper, while five tests were conducted for laminating plastic, and the results are shown in Figures 17 and 18, respectively. The Paper tends to be stiffer in MD and more ductile in CD, and the present results agree well with the expectation. However, for the laminating plastic, the 45° samples tend to be weaker but more

ductile than the other two directions. Note that the thin paper was loaded up to failure, and all the data after failure was removed in Figure 17. However, for the laminating plastic, it was only loaded up to 4% strain in all directions, and this was because the strains in the bi-axial tests were quite small; hence the calibration of up to 4% strain was deemed sufficient.

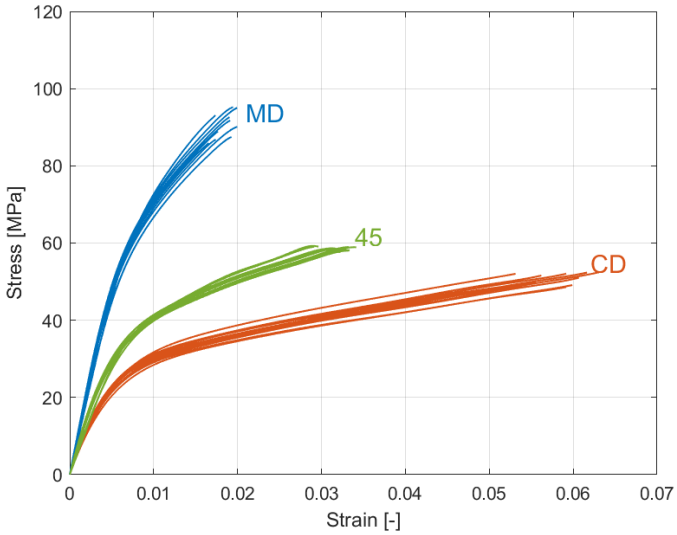


Figure 17: Experimental stress-strain curve for the paper in the different material directions.

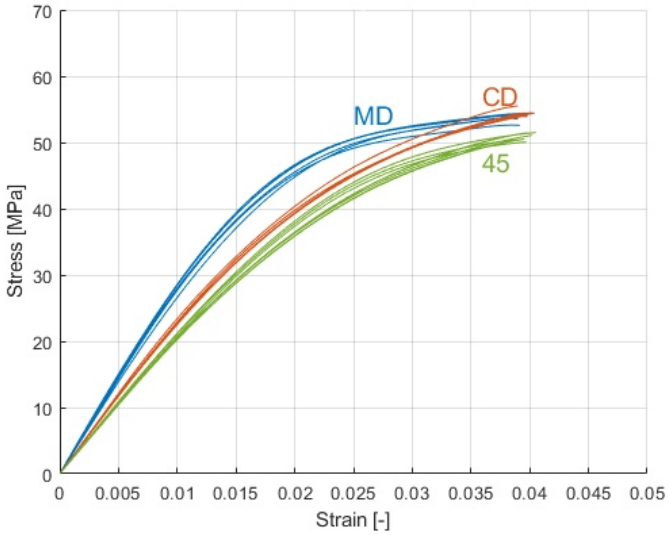


Figure 18: Experimental stress-strain curve for the laminating polymer in the different material directions.

The Hill model calibration was performed on the experimental results' mean value.

The material properties needed for the Hill model calibration were the in-plane elastic, plastic properties, and anisotropic yield stress ratios. The elastic properties were obtained from the experimental stress-strain curve and are listed in Table 3.

Table 3: Elastic properties of the paper and the polymer

| **Material** | $E_{xx}$ **[MPa]** | $E_{yy}$ **[MPa]** | $G_{xy}$ **[MPa]** | $\nu_{xx}$ **[-]** |
|---|---|---|---|---|
| **Paper** | 10573 | 6420 | 2362 | 0.38 |
| **Plastic** | 2943 | 2374 | 745 | 0.33 |

The plastic parameters of the Hill model were obtained by curve fitting the simulation results with experimental results. These material parameters, which gave a good fit to the experimental results, are listed in Table 4.

Table 4: Plastic properties of the paper and the polymer

| **Material** | $\sigma_0$ **[MPa]** | $H_0$ **[MPa]** | $n$ **[-]** | $R_{xx}$ **[-]** | $R_{xy}$ **[-]** |
|---|---|---|---|---|---|
| **Paper** | 9.7 | 98 | 3.55 | 2.7 | 2 |
| **Plastic** | 10 | 90 | 6 | 1.005 | 0.86 |

It can be seen in Figures 19 and 20 that the Hill material model fits the experimental results well for the paper and the polymer, respectively.

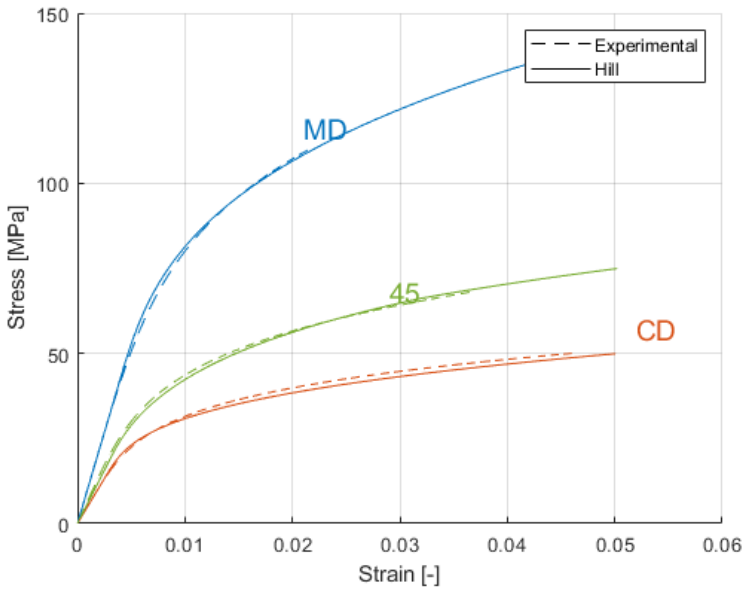


Figure 19: Experimental stress-strain curve fitted with the Hill model in the different material directions.

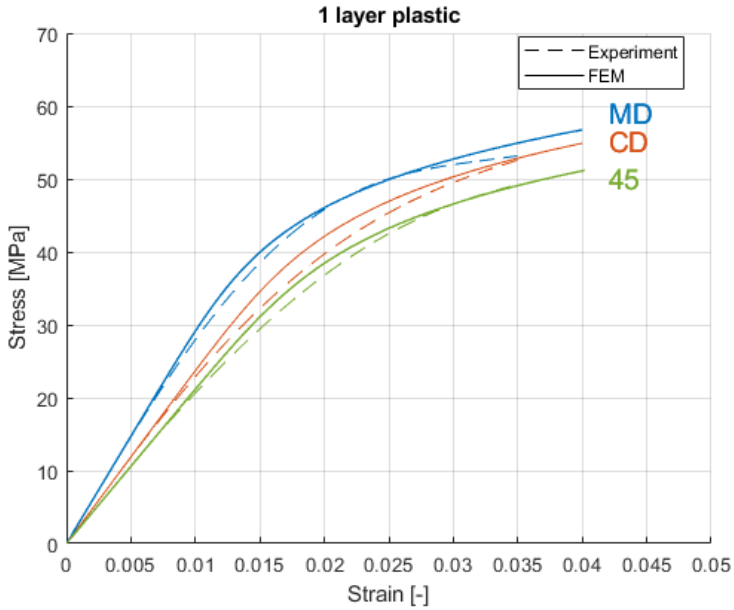


Figure 20: Experimental stress-strain curve fitted with the Hill model in the different material directions.

## 5.3 Bi-axial test simulation

The bi-axial tests were simulated using the calibrated material model for paper and laminating plastic. The force vs. displacement for the different load cases for both the experimental and the FEM results, respectively, are plotted in Figures 21-23.

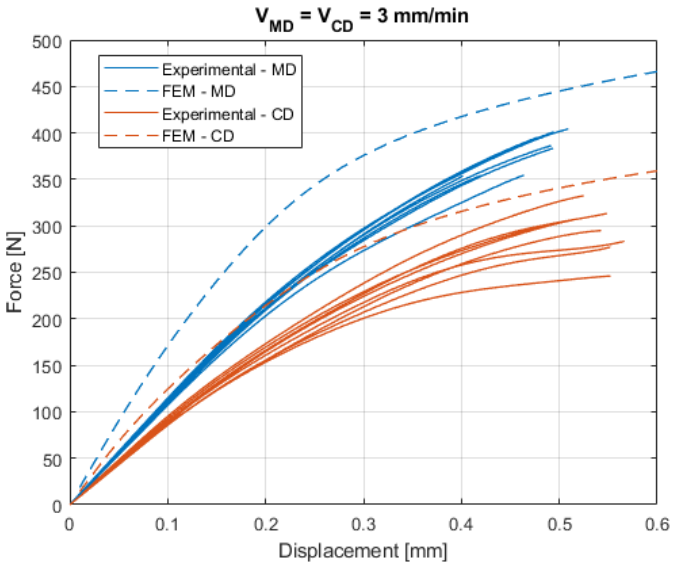


Figure 21: Comparison between FEM and experimental results when the displacements are equal in MD and CD.

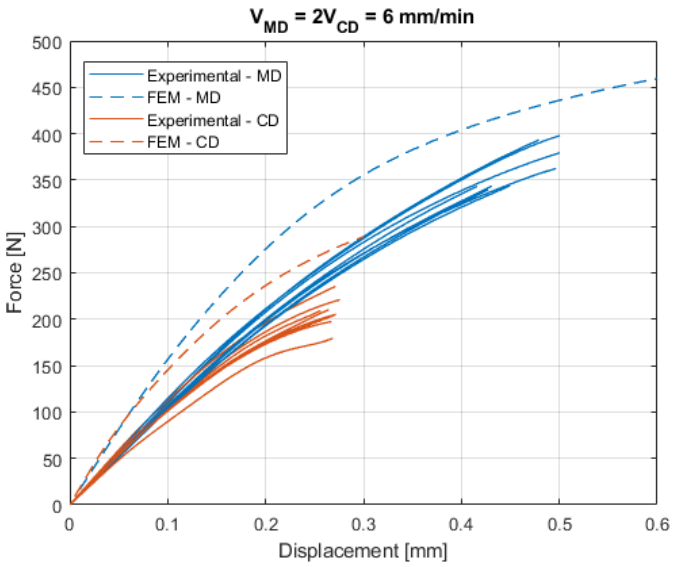


Figure 22: Comparison between FEM and experimental results when the displacements are twice as large in MD than in CD.

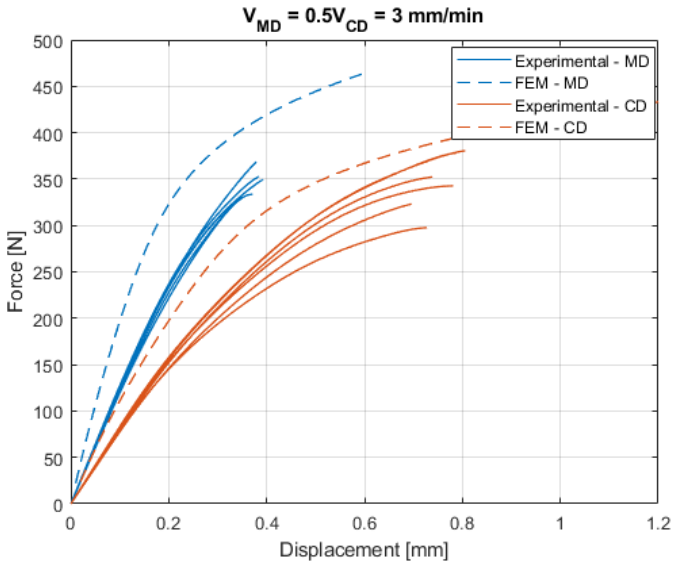


Figure 23: Comparison between FEM and experimental results when the displacements are twice as large in CD than in MD.

DIC analyses were performed, and the results are presented below. The directional displacements in MD and CD for the two points shown in Figure 10 from DIC and FEM for the different load cases are plotted in Figures 24-26.

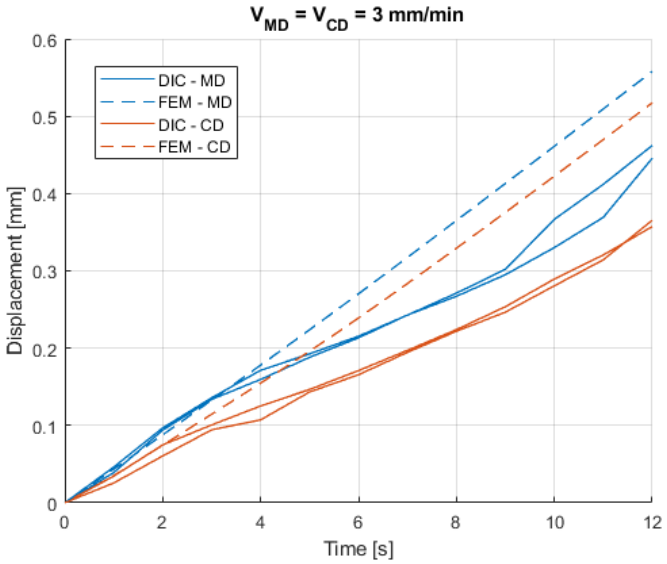


Figure 24: Displacement vs. time when the displacements are equal in MD and CD.

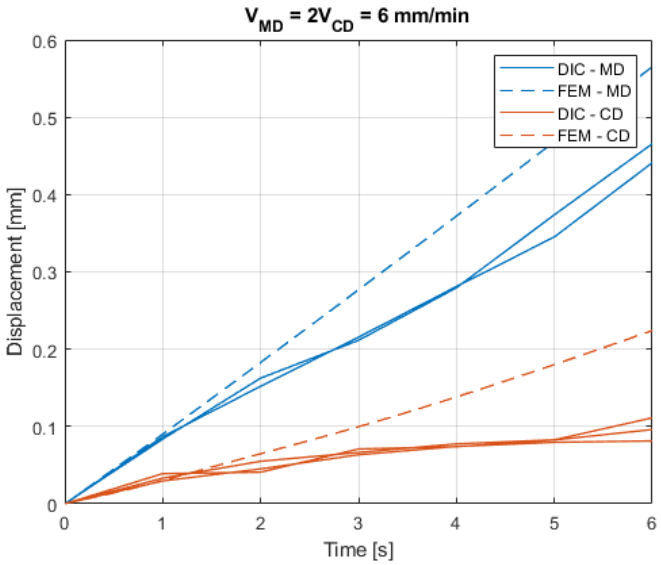


Figure 25: Displacement vs. time when the displacements are twice as large in MD than in CD.

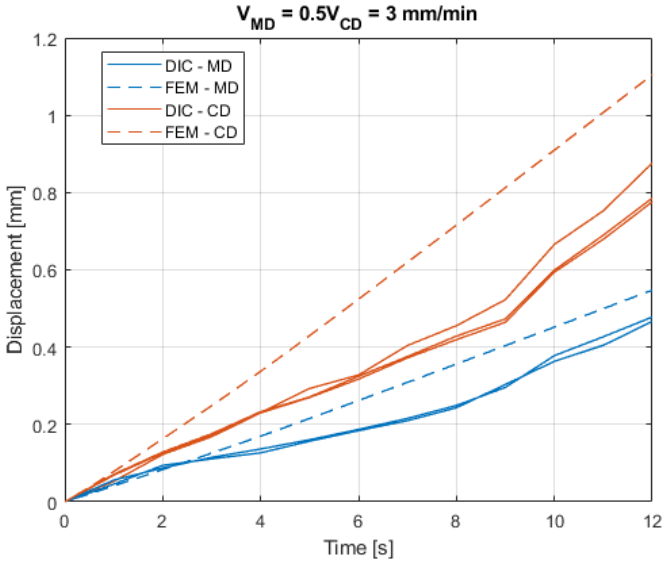


Figure 26: Displacement vs. time when the displacements are twice as large in CD than in MD.

A uniaxial tensile test and simulation were also conducted on laminated paper. The test was done on two different setups; the only difference was the width of the specimen. Specimens of widths 15 and 30 mm were used. The results of the stress-strain curve, from experiments and simulations, are plotted in Figures 27 and 28.

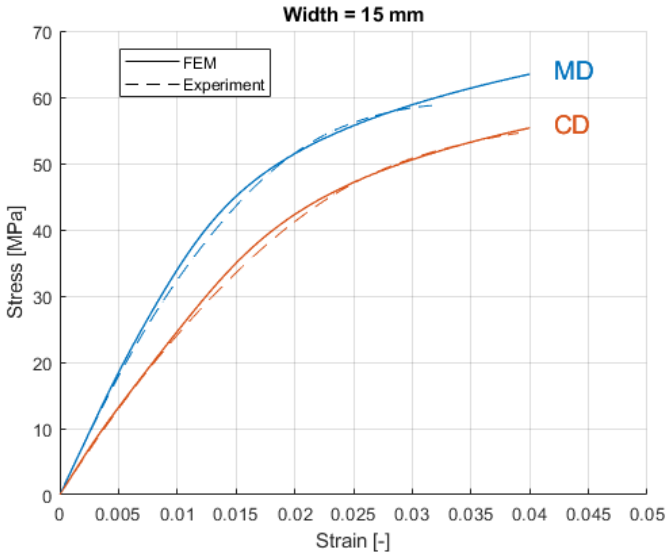


Figure 27: Uniaxial tensile test on 15 mm wide laminated paper.

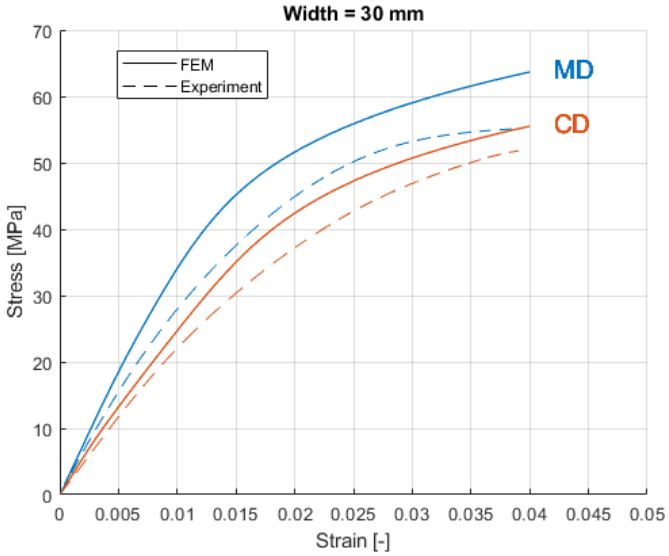


Figure 28: Uniaxial tensile test on 30 mm wide laminated paper.

# 6 Discussion

It is desired to have failure initiate in the central region where the deformation and loading are bi-axial. To overcome this challenge, a new bi-axial specimen was proposed and implemented. In almost all the specimens tested, failure initiation and total failure occurred more or less simultaneously. Hence, in most cases, it was difficult to capture where failure initiated because the camera used to record the test had too low frame-rates per second. However, failure initiation was captured in some tests; for those cases, it always initiated in the central region, as illustrated in Figure 14. In addition, the failure propagated at a certain angle depending on the load case, as shown in Figure 16. The small variation can be explained by the material's imperfection, such as inhomogeneously distributed fibers, uneven surface, etc. Nevertheless, failure initiation, failure propagation, limit force, and limit deformation, among other things, were very systematic and showed good reproducibility, indicating that the designed specimen was successful. Therefore, it can be used to perform bi-axial tests on thin paper, which otherwise would have failed at the clamps or the notches.

Since paper is temperature and moisture-dependent, the material properties of the paper might be affected by the lamination process where the temperature was set to 100 °C. To see the effect of the lamination process, uniaxial tests were conducted on a $100 \times 15$ mm paper specimen that passed through the laminating machine. The specimens were kept overnight in a climate-controlled environment before the test. As seen in Appendix A, the material properties of the paper were not affected by the lamination process as long as they were kept in a climate-controlled environment after the lamination process. Therefore, all the bi-axial specimens were kept overnight in a climate-controlled environment before the test to ensure that the bi-axial results were not affected by the lamination process.

The Hill material model captures the material behaviour of the paper very well, both during the elastic and the elasto-plastic regimes. However, unlike the paper, the model captures the elastic behaviour of the laminating plastic very well, but some deviations are observed in the plastic region. This is because the hardening response of the material model is the same in all directions, which is governed by the hardening behaviour of the reference direction. However, from the experimental results, the hardening behaviour of the plastic in MD and CD are different; hence, the model could not capture the material behaviour as well as it does for

the paper. However, this small deviation, was deemed acceptable because they are small and because the main region of interest was in the center of the specimen, which only consisted of paper.

Looking at Figure 21, it can be observed that the results from FEM behaves in a similar manner in both directions. However, the FEM results are stiffer and overestimate the experimental results in overall. This behaviour is repeated for the other two load cases, as seen in Figures 22 and 23. However, the FEM results captures the behaviour but overestimate the forces in all the load cases analyzed. This implies, for instance, that there must be some systematic error. One systematic error that can cause this kind of deviation is slippage at the clamps. Slippage is hard to avoid entirely, but it can be considered by back-fitting the boundary condition used in the simulations. This is done by prescribing the displacements in the FE model so that elements at the same locations of the tracking squares in Figure 10 have the same displacements as those obtained from DIC. The deviation might also have originated from the modelling of the bi-axial specimen. For instance, the modelling using layered section to model the specimen might have been an inaccurate way to simulate the experimental tests. It might also have been a combination of both.

To eliminate slippage as a possible source of error, DIC was performed. As expected, it is shown in Figure 24 that slippage did exist at both clamps, but more interesting is what happened in the first three seconds. In these first three seconds, the displacemet from DIC and simulation are equal, meaning there was no slippage in the beginning when loads were equal in both directions. A Similar pattern, i.e., no slippage at the beginning can be observed for the other two cases, as illustrated in Figures 25 and 26. Let us take a closer look at the case of equal displacement in MD och CD, at three seconds, the applied displacement at the clamps was 0.15 mm, which means that the deviation, at least in the elastic region, can not be explained by slippage.

If there is no slippage during the first three seconds, the modelling using three layered shell elements had to be double-checked to see if it is the correct way to do it. In Figure 27, uniaxial tensile tests results for the laminated paper were compared with the previous model. As seen in the plot, the results from the simulation match the experimental results. Hence, this eliminates modelling the specimen, as three layered shell elements, as a possible source of error. Moreover,

the problem cannot be in the material model itself since it is proven by Alzweighi's previous work [3] that the model can handle more complicated loads cases. Now the question remains, how accurate were the DIC results? DIC results are sensitive, especially when displacements are very small. Lighting exposure, out-plane deformation, and error in scale calibration are among other issues that can disturb the DIC results. Hence, it is reasonable to question the DIC results.

A simple uniaxial test was performed to deduce if the DIC result were inaccurate. Slippage is dependent on the contact surface and resistance force. Increasing the width of the uniaxial specimen increases the resistance force, which in turn increases the risk of slippage. As shown in Figure 28, when the width was increased to 30 mm, the experimental results deviated from the FEM results. Slippage at larger forces was expected but as seen in Figure 28, the experimental results were less stiff even in the beginning, which means slippage did occur even in the initial parts of the test. The bi-axial specimen was of the same dimension at the clamp as the wide uniaxial test and twice as short, meaning the resistance force would be higher. Therefore, if slippage occurred already in the uniaxial test, the risk of slippage occurring at bi-axial tests was even higher. This indicates that there was slippage at the beginning which was not captured by comparing FEM results and DIC. It can also be observed that the deviation between FEM and experimental results in the uniaxial and bi-axial tests was similar, which further supports the assumption that slippage was the reason the FEM results deviated from the experimental results in the bi-axial tests.

Although slippage is hard to avoid entirely, it can be minimized. For example, the clamps used in this experiment had a rough surface, but changing it to a smother surface can increase the contact surface, leading to better grip. Moreover, by changing the surface of the clamp from metal to plastic, friction force can be increased, since the friction coefficient for plastic on plastic is higher than plastic on metal. Furthermore, to exclude the slippage factor better DIC setup can be implemented. For example, a telecentric camera lens can be used, so possible out-plane deformations don't affect the DIC results. Moreover, a better lighting system can be used to avoid regions with over-exposures which in turn will affect the DIC results.

# 7 Conclusion and Future work

## 7.1 Conclusion

The cruciform shape of the thin paper in the test specimen leads to fracture in the clamped or notch region when exerted to bi-axial loading in an experimental test equipment. However, failure in the arms of the cruciform, can be avoided by strengthening the arms of the thin paper. This is simply done by laminating, on both sides with one sheet of polymer material, the cruciform-shaped paper everywhere but in the central region where there is a bi-axial stress state. The specimen designed in this project was tested and produced a systematic and repetitive fracture in the central region for different load cases. This indicates this specimen can be used to conduct bi-axial testing, i.e. multi-axial material characterization of thin paper.

Hill material model reflects the anisotropic behaviour of paper very well and can be used to model the paper in FE simulations. Even though the generally higher values in the FEM result compared to the experiment, the FE-model did capture the observed behaviour well. Moreover, the deviation was explained by slippage at the clamps, which could be captured by DIC.

## 7.2 Future work

- Slippage is generally one of the main concerns during tensile testing of a stiff and smooth material, like laminated plastic. Therefore, a better set of clamps should be used to minimize slippage at the clamps.
- It is hard to prevent slippage entirely. Therefore, a better DIC setup has to be used to capture the small slippage at the clamps. The DIC results can later be used to optimize the FEM result.
- For the different load cases studied, the specimen had different failure orientations, which indicates there must be some driving force. This can be studied in future work to better understand the material anisotropic failure behaviour.
- Damage mechanics should be included in the FEM model. Thus, the failure orientation seen in the experiment can be used for a better choice of material model.

# References


[1] Ansys Workbench Users Manual. (2020). Version 2020R2. ANSYS, Inc., 275 Technology Drive Canonsburg.

[2] Alexandersson, M. (2020). *Macroscopic modelling of coupled multiphysics in swelling cellulose based materials*, PhD thesis, Lund University.

[3] Alzweighi, M.,Mansour, R., Tryding, J., Kulachenko, A. (2021). Evaluation of Hoffman and Xia plasticity models against bi-axial tension experiments of planar fiber network materials. *International Journal of Solids and Structures*, 238. 111358. 10.1016/j.ijsolstr.2021.111358.

[4] Baum,G.A., Brennan, D.C., Habeger, C.C. (1981). Orthotropic Elastic Constants of Paper. *Tappi Journal*, 64(8), pp. 97-101.

[5] de Ruvo A., Carlsson L., Fellers C. (1980). The biaxial strength of paper. *Tappi Journal*, 63(5), 133–136.

[6] Gunderson D., Rowlands R. (1983). Determining paperboard strength - biaxial tension, compression, and shear. *Proc. Int. Paper Phys. Conf.,* pp 253–263.

[7] Karlsson, H. (2007). *Some aspects on strength properties in paper composed of different pulps*, Licentiate dissertation, Karlstad University.

[8] LaVision, F.o.i. (2010). Digital image correlation (DIC).

[Online]. Available: `https://www.lavision.de/en/techniques/dic-dvc/index.php` [Accessed: 23-04-2022].

[9] Lekhnitskii, S,. (1981). Theory of Elasticity of Anisotropic Body. Mir Publishers.

[10] Linvill, E., Östlund, S. (2012). Biaxial In-Plane Yield and Failure of Paperboard. *Nord. Pulp Paper Res. J.,* 31(4), pp. 659–667, 2016.

[11] MATLAB documenation (2020). Version R2020b. The MathWorks, Inc., Natick, Massachusetts, United States.

[12] Niskanen, K. (2012). *Mechanics of Paper products.*

[13] Ottosen, N. S., Ristinmaa, M. (2005). *The Mechanics of Constitutive Modeling.* Elsevier, Lund

[14] Rundh, B. (2016). The role of packaging within marketing and value creation. *British Food Journal*, 118(10), pp. 2491–2511, 2016. doi: 10.1108/ BFJ-10-2015-0390.

[15] Schreier, H., Orteu, J-J., Sutton, M.a. (2009). Frontpage. *Image Correlation for Shape, Motion and Deformation Measurements. Basic Concepts, Theory and Applications,* pages ii–xx.

[16] Tryding, J. (1996). *In-Plane Fracture of Paper*. PhD thesis, Lund University.

[17] VIC-2D Users Manual. (2021). Version v6. Correlated Solutions, Inc. Irmo, South Carolina, USA

# Appendix A - Experimental results

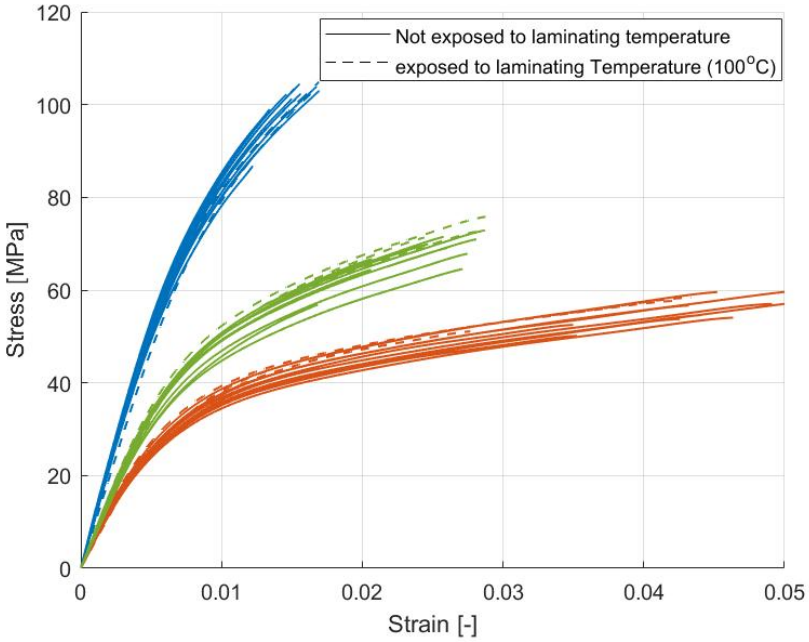


Figure 29: Stress-strain curves for thin paper.

# Appendix B - Failure orientations

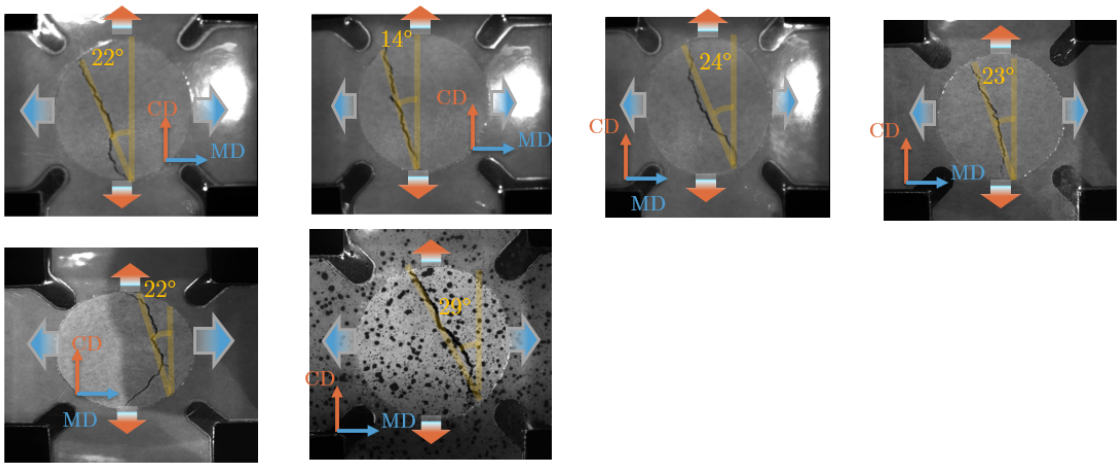


Figure 30: Crack angles for different biaxial tests for the case when displacements are equal in MD and CD.

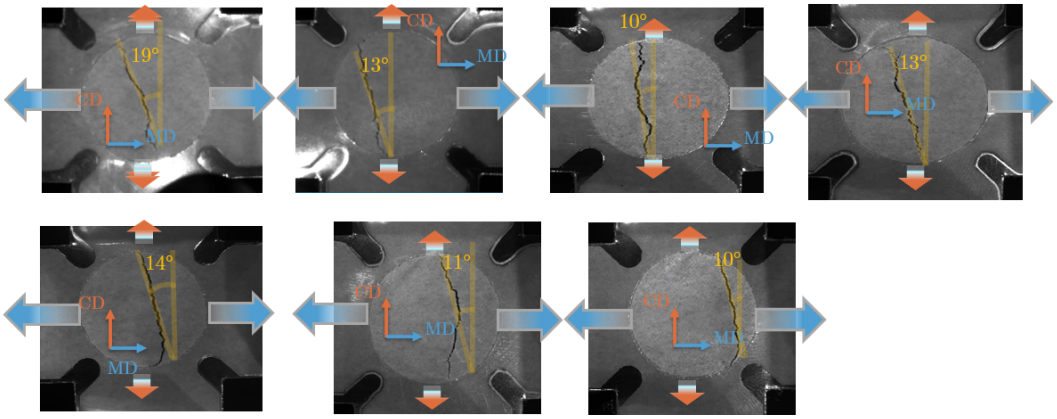


Figure 31: Crack angles for different biaxial tests for the case when displacements are twice as large in MD than in CD.

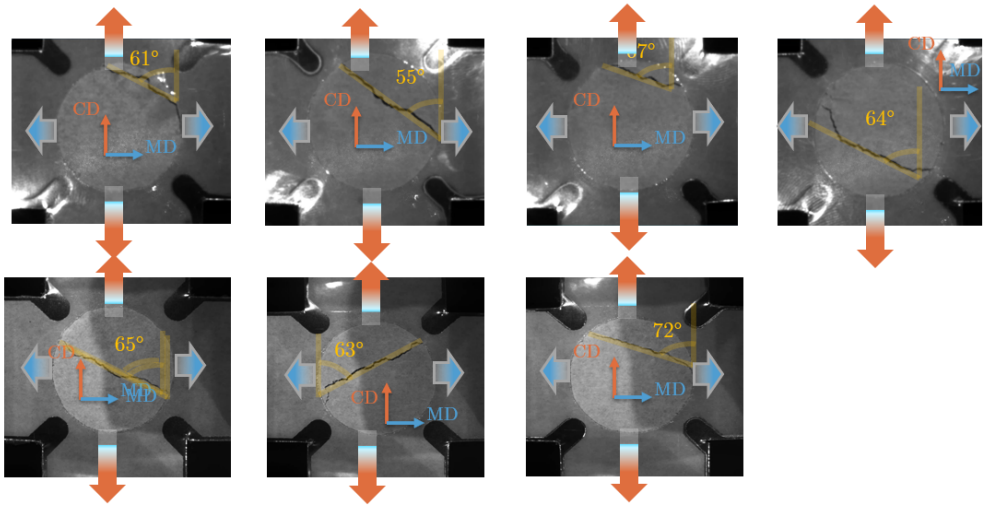


Figure 32: Crack angles for different biaxial tests for the case when displacements are twice as large in CD than in MD.

TRITA – SCI-GRU 2022:276